

## Supporting Information

### Role of water in dual-ionic pyrazolium salt promoted conversion of CO<sub>2</sub> at atmospheric pressure and room temperature

Danning Zheng,<sup>†a,b</sup> Fang Liu,<sup>†a</sup> Tengfei Wang,<sup>a</sup> Zhengkun Zhang,<sup>a</sup> Hans Ågren,<sup>a</sup>

Jinglai Zhang,<sup>\*a</sup> Mårten S. G. Ahlquist,<sup>\*c</sup> Li Wang<sup>\*a</sup>

*<sup>a</sup>Henan Province Engineering Research Center of Green Anticorrosion Technology for Magnesium Alloys, Henan University, Kaifeng, Henan 475004, PRChina; Henan Engineering Research Center of Corrosion and Protection for Magnesium Alloys, Henan University, Kaifeng, Henan 475004, PRChina; College of Chemistry and Chemical Engineering, Henan University, Kaifeng, Henan 475004, PRChina*

*<sup>b</sup>Key Laboratory of Tropical Translational Medicine of Ministry of Education, Hainan Provincial Key Laboratory for Research and Development of Tropical Herbs, Haikou Key Laboratory of Li Nationality Medicine, School of Pharmacy, Hainan Medical University, Haikou 571119, PR China*

*<sup>c</sup>Department of Theoretical Chemistry & Biology, School of Biotechnology, KTH Royal Institute of Technology, 10691 Stockholm, Sweden*

---

\*Corresponding authors.

E-mail addresses: [chemwangl@henu.edu.cn](mailto:chemwangl@henu.edu.cn) (L. Wang), [zhangjinglai@henu.edu.cn](mailto:zhangjinglai@henu.edu.cn) (J.L. Zhang), [ahlqui@kth.se](mailto:ahlqui@kth.se) (M.S.G. Ahlquist)

<sup>†</sup>These authors contributed equally to this work.

## 1. General Information

The CO<sub>2</sub> (99.9%) was obtained from Kaifeng Tengzongsheng Trading Co. Ltd.. Epoxides were purchased from Shanghai Macklin Biochemical Co. Ltd.. 1,1,3,3-tetramethylguanidine (TMG) was purchased from Tianjin Heowns Biochemical Technology Co. Ltd.. Methanol and ethyl acetate were all analytical grade and purchased from Tianjin Fuyu Fine Chemical Co. Ltd. All of reagents were used directly without further purification.

<sup>1</sup>H NMR (400 MHz) spectrum was tested with the spectral width of 20 ppm and the scan number of 16. Both <sup>1</sup>H NMR (400 MHz) and <sup>13</sup>C NMR (101 MHz) spectra were measured in Deuterium oxide (D<sub>2</sub>O) on a Bruker AVANCE III HD spectrometer. Fourier transform infrared spectroscopy (FT-IR) was recorded on Bruker vertex 70 using KBr pellets. Mass spectra (MS) were determined by Bruker Amazon SL mass spectrometer. GC analyses were carried out by Agilent GC-7890 B with flame ionization detector. The thermal decomposition temperature was analyzed with thermal gravimetric analyzer (TGA) (Mettler Toledo TGA/SDTA851e).

## 2. Experimental Section

### 2.1 The procedures for preparation of the dual-ionic pyrazolium salts.

First, all three dual-ionic pyrazolium salts were prepared through neutralization reactions.<sup>1</sup> As an example, the procedure for the preparation of [TMGH<sup>+</sup>][O<sub>2</sub>MEPZ<sup>+</sup>][Br<sup>-</sup>] (ILPT) was described. Methanol (10 mL), TMG (10 mmol, 1.1518 g), and CMEPzBr (10 mmol, 2.3508 g) were loaded into a 50 mL flask in a water bath of 30 °C with stirring. The neutralization reaction was allowed to proceed at room temperature for 12 h. The solvent was removed by rotary evaporation under vacuum at 40 °C. After that, acetonitrile (3 mL) and ethyl acetate (15 mL) was added to the residue. Then, they were refrigerated for 10 hours. Finally, the light yellow solid with

more than 99% purity was obtained as target product.

### 2.1.1 Characterization of the dual-ionic pyrazolium salts

**ILPT**: light yellow solid, melting point, 144 °C-145 °C. <sup>1</sup>H NMR (400 MHz, D<sub>2</sub>O) δ 8.10 (s, 1H), 8.00 (s, 1H), 6.64 (m, 1H), 4.95 (s, 2H), 4.19 (q, J = 7.3 Hz, 2H), 2.77 (s, 12H), 1.38 (t, J = 7.3 Hz, 3H). <sup>13</sup>C NMR (101 MHz, D<sub>2</sub>O) δ 170.52, 161.34, 138.15, 136.20, 107.74, 52.65, 45.47, 39.17, 13.26. MS (ESI): [-O<sub>2</sub>MEPZ<sup>+</sup>] m/z 154.65, [TMGH<sup>+</sup>] 115.84. Anal. Calcd for C<sub>12</sub>H<sub>24</sub>N<sub>5</sub>O<sub>2</sub>Br: C, 41.15, N, 20.00, H, 6.91. Found: C, 40.84, N, 19.66, H, 6.825. (See Fig. S1)

[TMGH<sup>+</sup>][-O<sub>2</sub>PHIm<sup>+</sup>][Br<sup>-</sup>] (**ILW**) [1]: white solid, melting point: 111 °C-112 °C <sup>1</sup>H NMR (400 MHz, D<sub>2</sub>O) δ 8.71 (d, J=1.6 Hz, 1H), 7.52 (d, J=1.8 Hz, 1H), 7.46 (d, J=1.7 Hz, 1H), 4.26 (t, J=7.0 Hz, 2H), 2.23 (t, J=6.9, 1.4 Hz, 2H), 2.14 (m, 2H). <sup>13</sup>C NMR (101 MHz, D<sub>2</sub>O) δ 180.97, 161.31, 134.59, 121.75, 120.03, 48.80, 38.96, 33.75, 26.30. MS (ESI): [-O<sub>2</sub>PIm] m/z 153.48, [TMGH<sup>+</sup>] 115.82. Anal. Calcd for C<sub>12</sub>H<sub>24</sub>N<sub>5</sub>O<sub>2</sub>Br: C, 41.15, N, 20.00, H, 6.91. found: C, 41.31, N, 20.54, H, 6.896. (See Fig. S2)

### 2.2 Typical procedure for the synthesis of cyclic carbonates

The catalytic process was conducted in a 50 mL high pressure stainless-steel autoclave. For a typical run, the ECH (5 mmol, 0.4626g) and **ILPT** (10 mol%, 0.175g) were added to the autoclave, then CO<sub>2</sub> was introduced into the autoclave to keep 0.1 MPa after the air evacuated. The autoclave was stirred at 30 °C or 50 °C and kept for 12 h or 6 h, respectively. Upon the completion of the reaction, the remaining CO<sub>2</sub> was released slowly. Meanwhile, the reactor was cooled to room temperature and the product was obtained by extraction with ethyl acetate and separation. The product in ethyl acetate phase was quantitatively analyzed on GC to determine the product yield.

### 2.3 Recyclability of the catalyst.

The following reactions were performed under 50 °C, 0.1 MPa CO<sub>2</sub> pressure (autoclave), 10 mol% **ILPT**, and 6 h. After each reaction, the mixture was removed from the reactor using methanol for dissolution, and solvent was evaporated. ECH and product can be dissolved in ethyl acetate, while **ILPT** is insoluble in ethyl acetate. Therefore, the **ILPT** was separated from the product by washing with ethyl acetate for three times. Finally, the **ILPT** was collected after concentrating the liquid. Then the catalyst was reused directly for another run.

#### **2.4 Mechanism experimental confirmation details.**

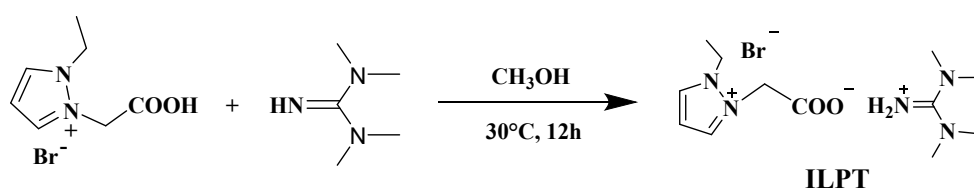
In a typical CO<sub>2</sub> capture experiment, 1.25 mmol of **ILPT** was loaded into a 50 mL autoclave with the stirrer, then, CO<sub>2</sub> was introduced into the autoclave and kept for 0.1 MPa pressure after the air evacuated. The autoclave was heated to 30 °C and kept for 2 h. Finally, the remaining CO<sub>2</sub> was released slowly and the sample (a) CO<sub>2</sub>+**ILPT** was obtained. From the above method, we obtained samples (b) CO<sub>2</sub>+ECH+**ILPT**, (c) CO<sub>2</sub>+H<sub>2</sub>O+**ILPT** and (d) CO<sub>2</sub>+ECH+H<sub>2</sub>O+**ILPT**, respectively. When the 5 mmol ECH, 1.25 mmol H<sub>2</sub>O and 1.25 mmol **ILPT** were loaded into autoclave and kept for 12 h, the sample (e) was obtained. The samples were characterized by NMR techniques. The <sup>13</sup>C NMR analyses were conducted in Deuterium oxide (D<sub>2</sub>O) on a Bruker AVANCE III HD (400 MHz, 101 MHz) spectrometer. The characterization results of the samples were present in Fig. 6.

Similarly, We also prepared another set of samples (a)-(f), and these samples were measured by Fourier transform infrared spectra (FT-IR) spectrometer. The characterization results of the samples were present in Fig. 7.

#### **2.5 Experimental details of the effect of rotary speed on yield**

The catalytic process was conducted in a 50 mL high pressure stainless-steel

autoclave with a magnetic stirring. For a typical run, the 5 mmol ECH, 1.25 mmol H<sub>2</sub>O and **ILPT** (25 mol%, 0.4375g) were added to the autoclave, then CO<sub>2</sub> was introduced into the autoclave to keep 0.1 MPa after the air evacuated. The autoclave was stirred at 30 °C and kept for 6 h, and the speed of rotation of autoclave was set from 0 rpm to 450 rpm, respectively. Upon the completion of the reaction, the remaining CO<sub>2</sub> was released slowly. Meanwhile, the reactor was cooled to room temperature and the product was obtained by extraction with ethyl acetate and separation. The product in ethyl acetate phase was quantitatively analyzed on GC to determine the product yield.



**Scheme S1** Preparation of the dual-ionic pyrazolium salt.

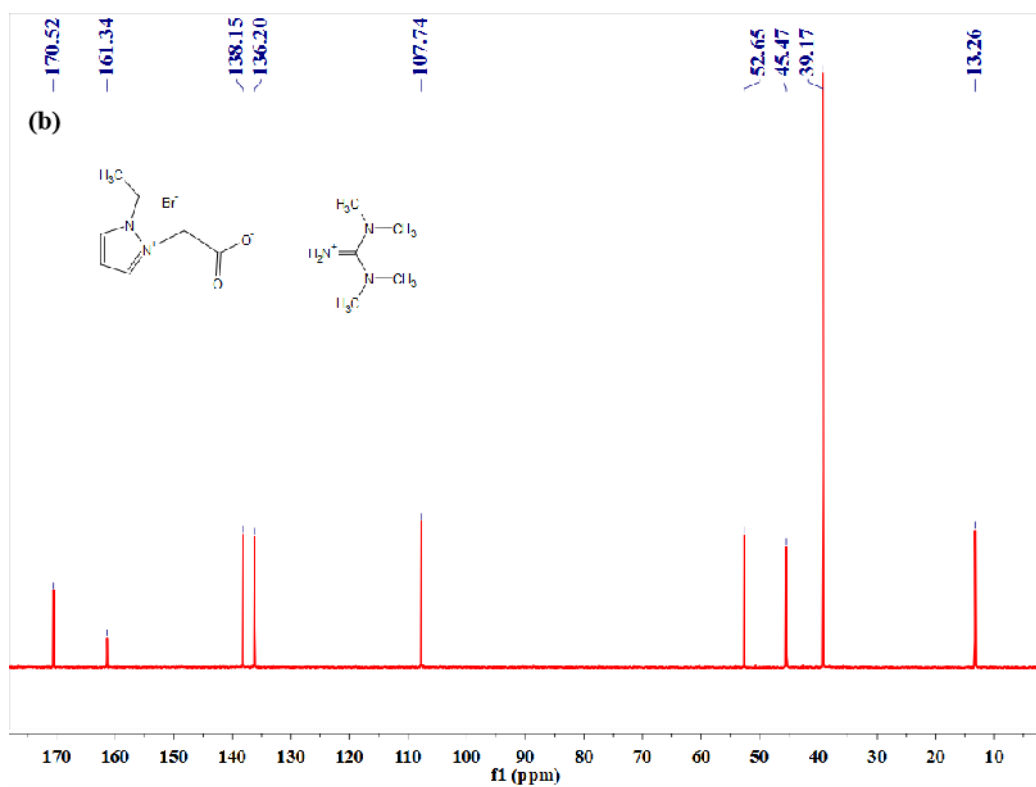
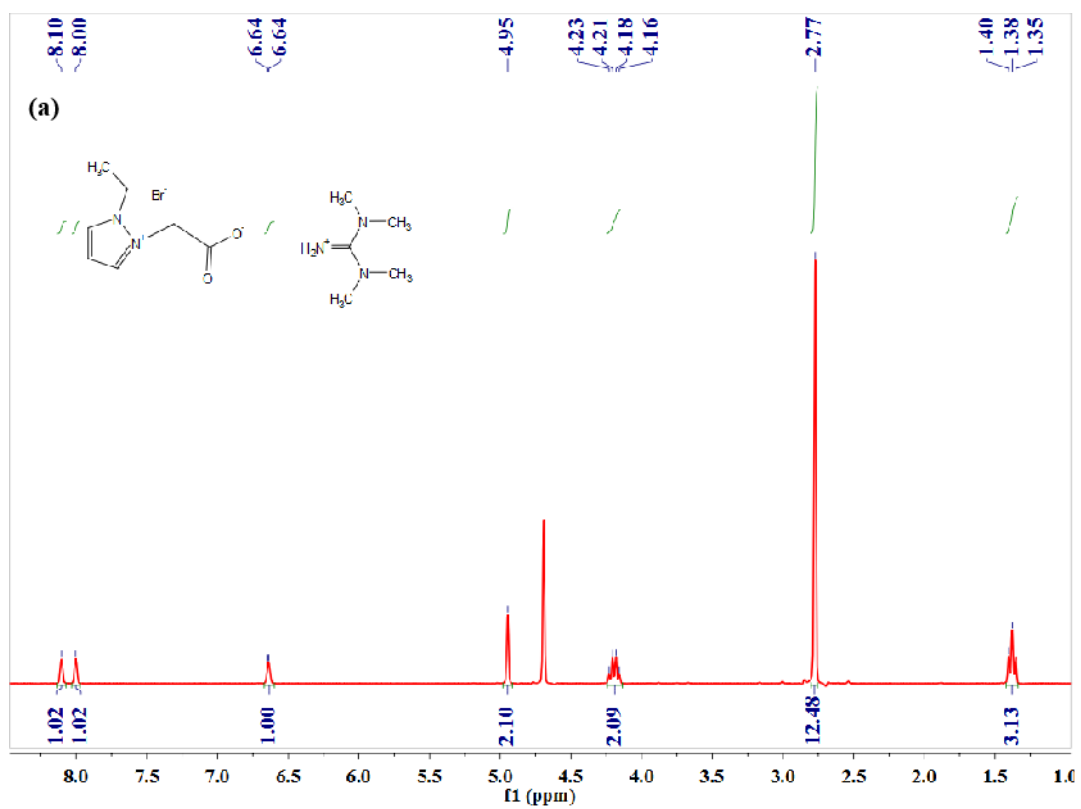


Fig. S1  $^1\text{H}$  NMR spectrum (a) and  $^{13}\text{C}$  NMR spectrum (b) of ILPT.

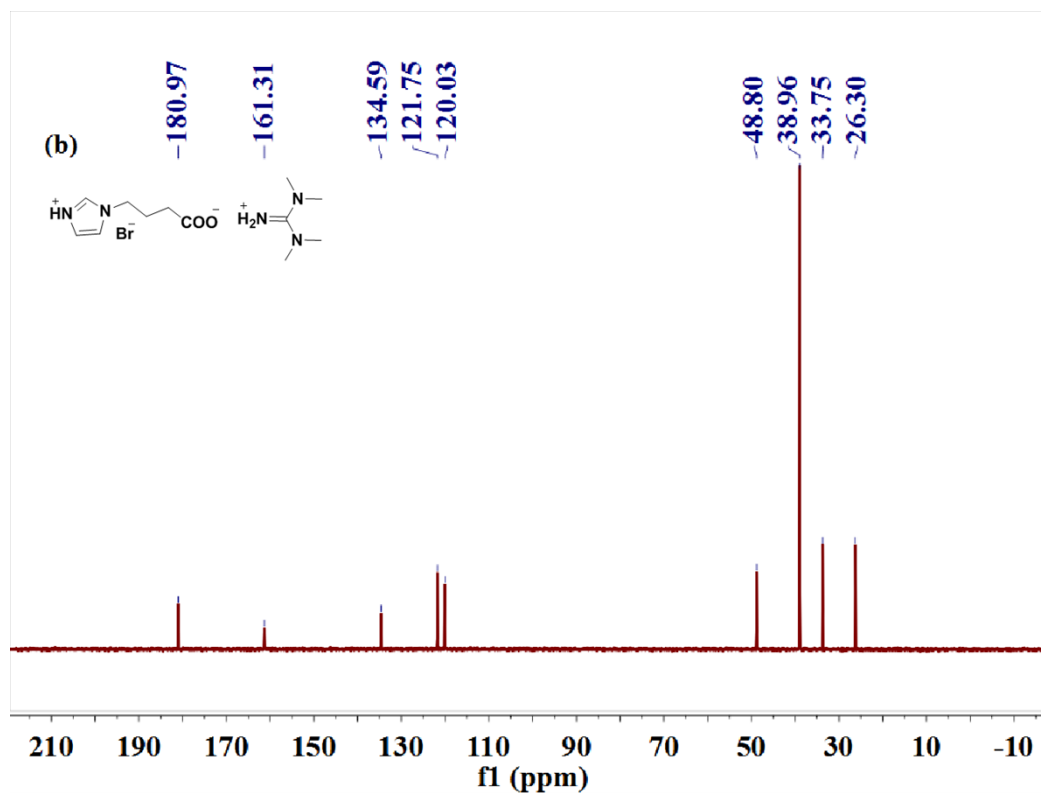
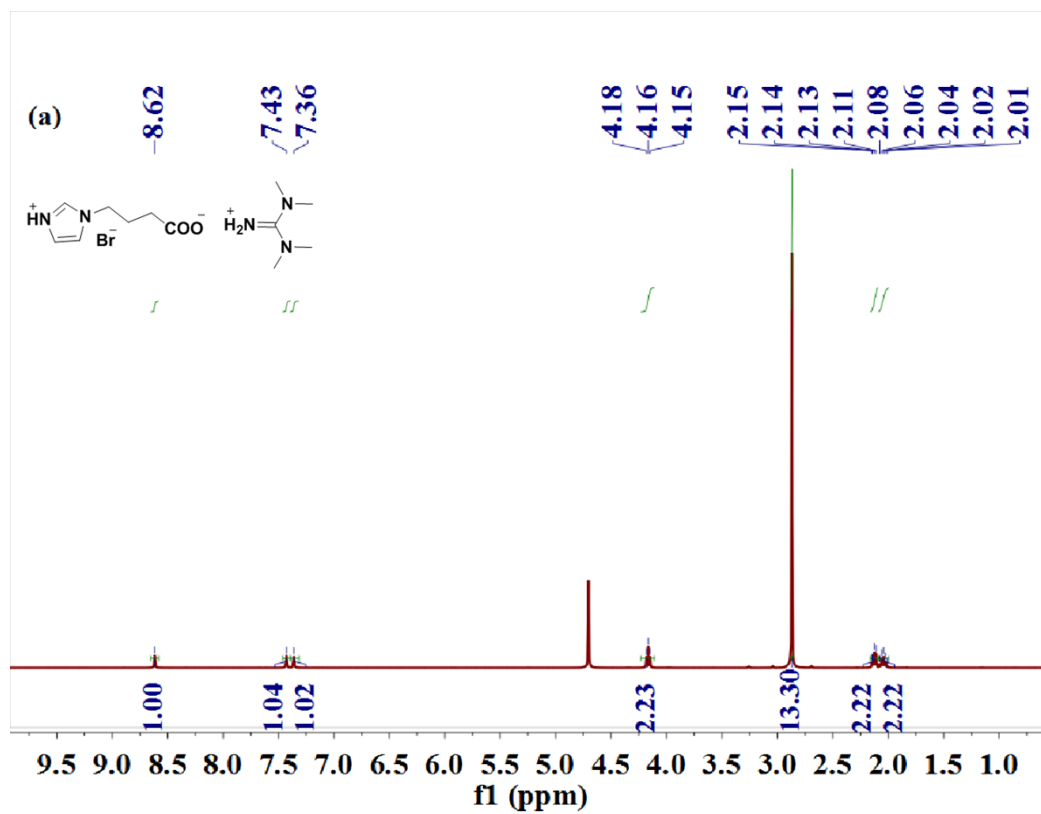
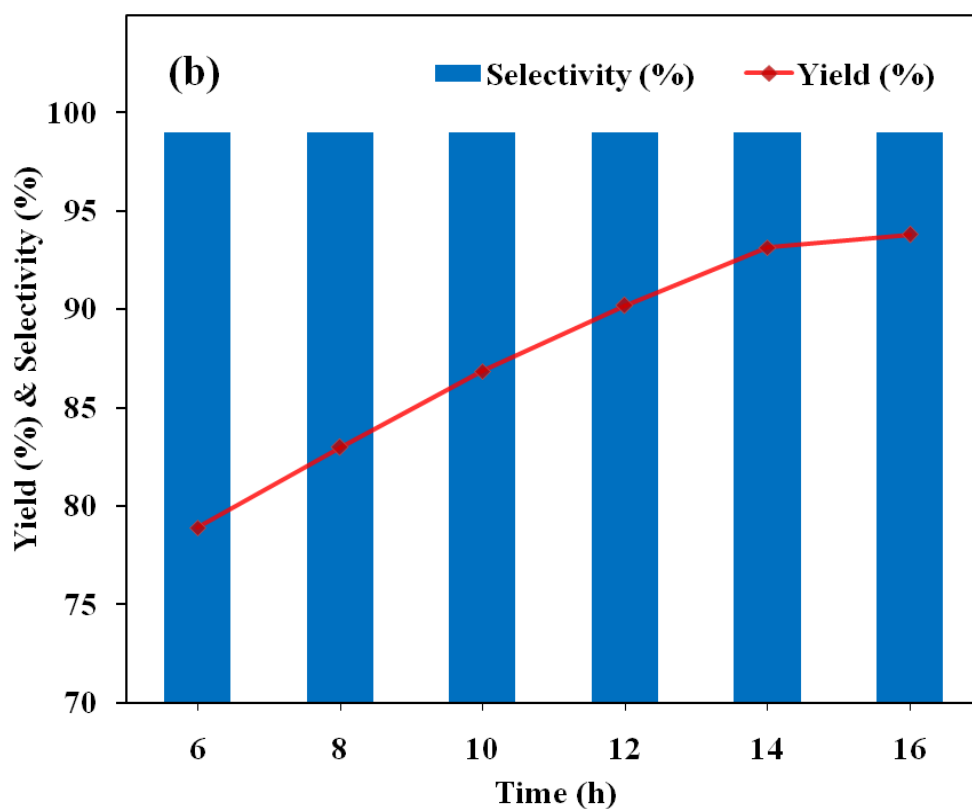
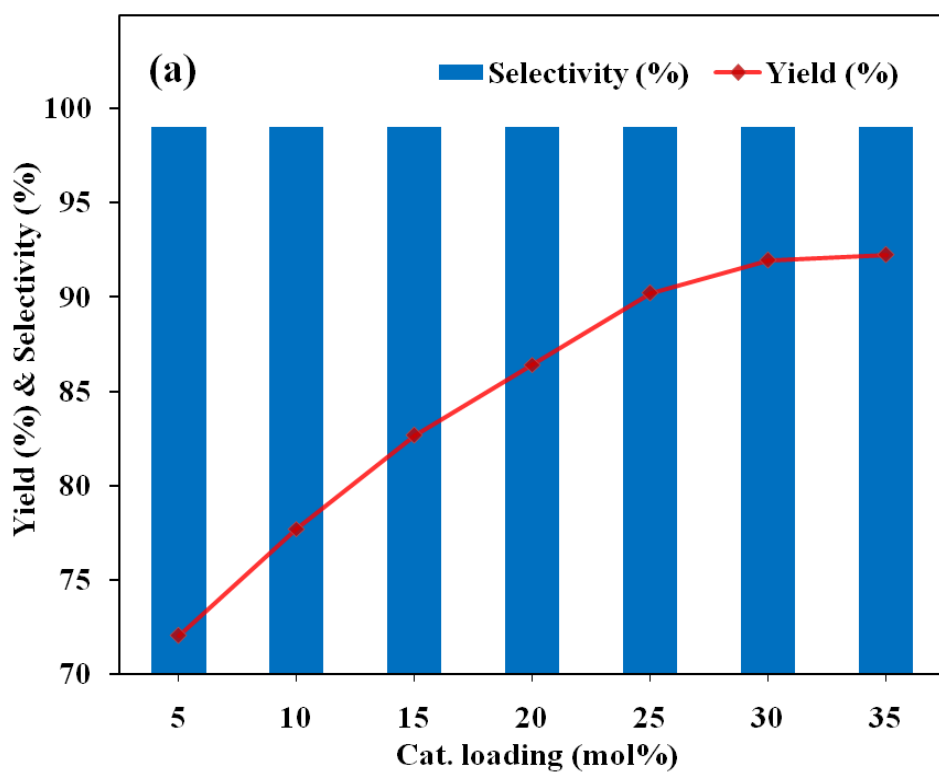
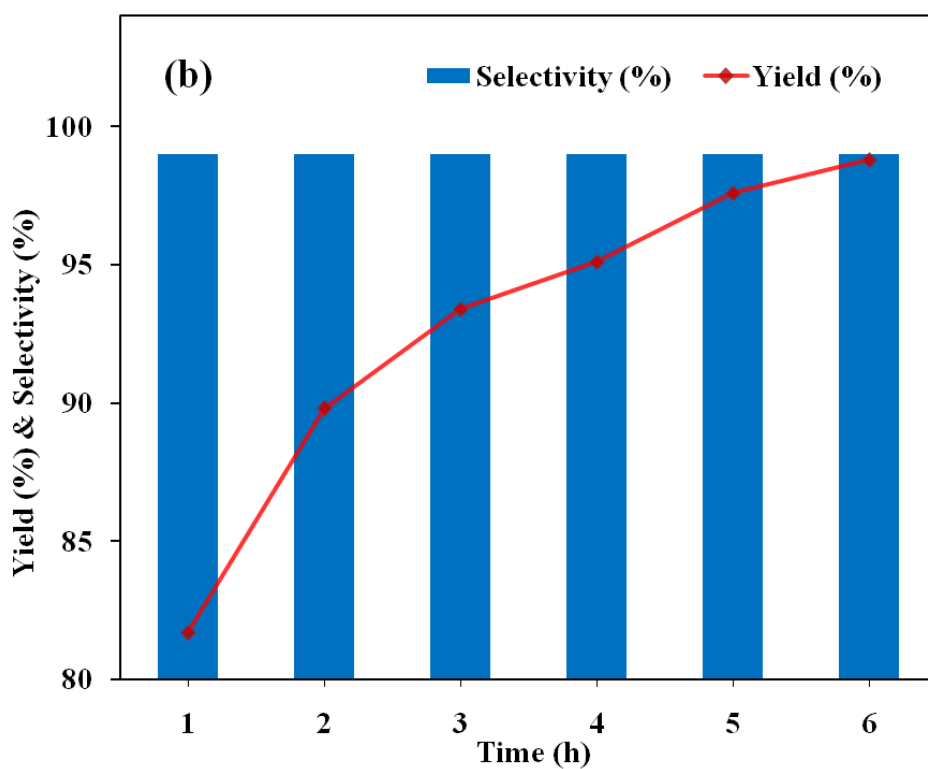
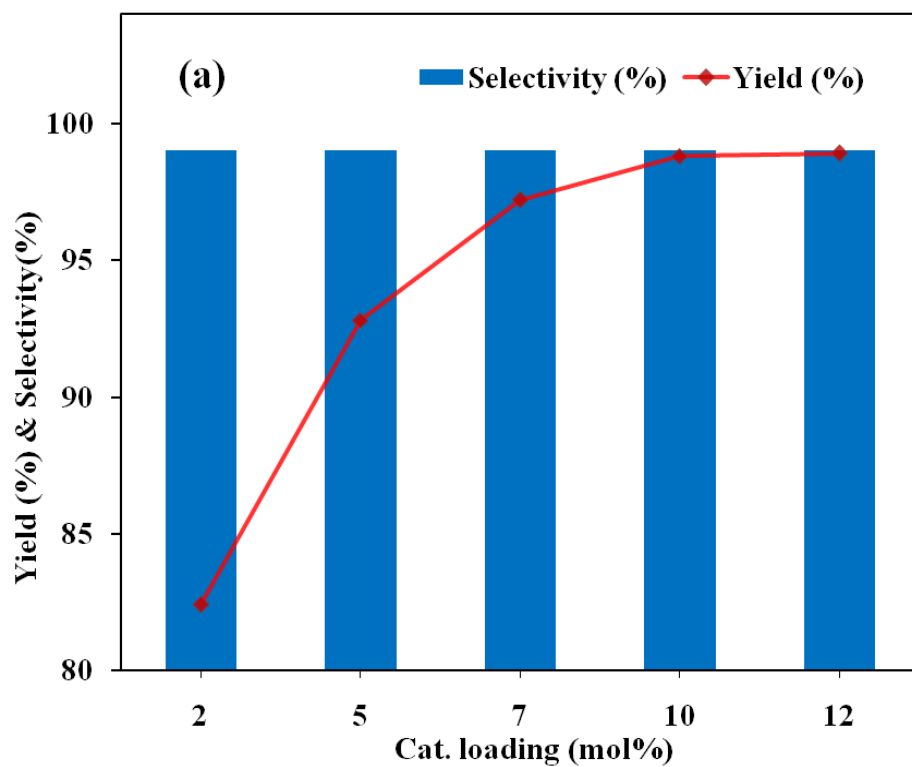


Fig. S2.  $^1\text{H}$  NMR spectrum (a) and  $^{13}\text{C}$  NMR spectrum (b) of ILW<sup>1</sup>



**Fig. S3** (a) The effect of catalyst amount on CPC yield: ECH 5 mmol, 30 °C, 0.1 MPa CO<sub>2</sub> (autoclave), and 12 h. (b) The effect of reaction time on CPC yield: ECH 5 mmol, 30 °C, 0.1 MPa CO<sub>2</sub> (autoclave), and 25 mol% catalyst dosage.





**Fig. S4 (a)** The effect of catalyst amount on CPC yield: ECH 5 mmol, 50 °C, 0.1 MPa CO<sub>2</sub> (autoclave), and 6 h. **(b)** The effect of reaction time on CPC yield: ECH 5 mmol, 50 °C, 0.1 MPa CO<sub>2</sub> (autoclave), and 10 mol% catalyst dosage.

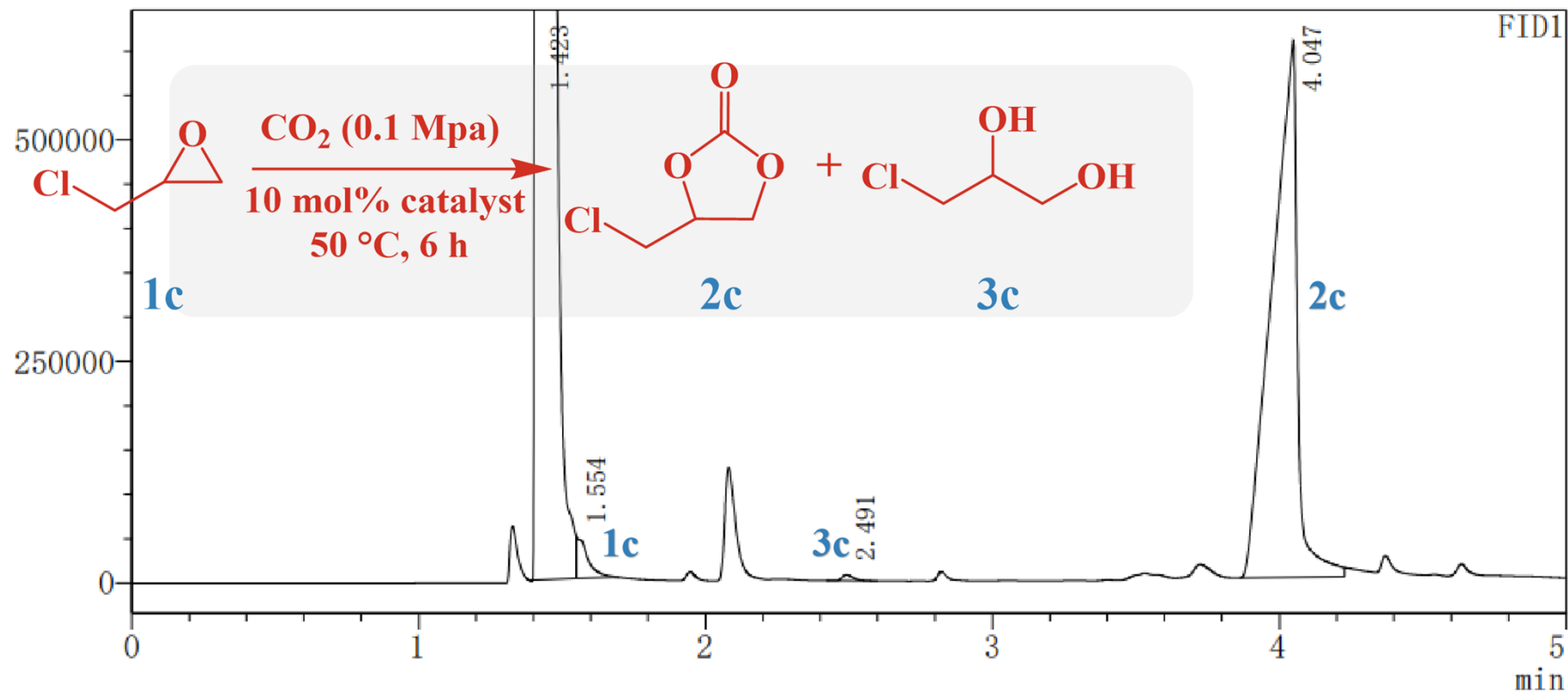
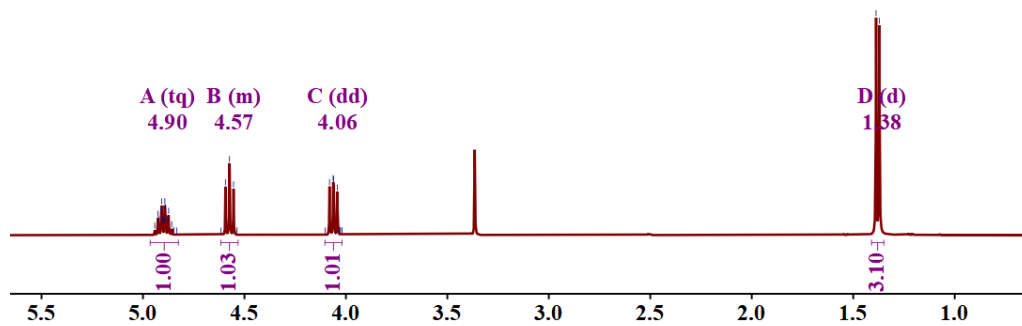
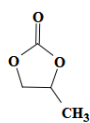
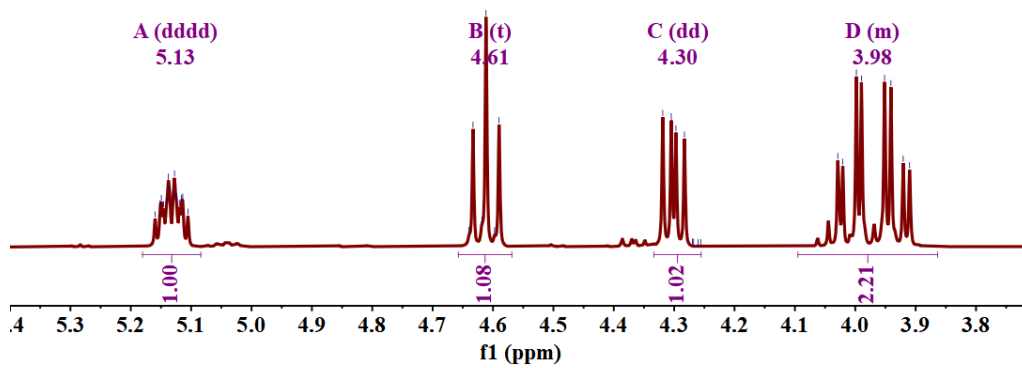
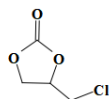
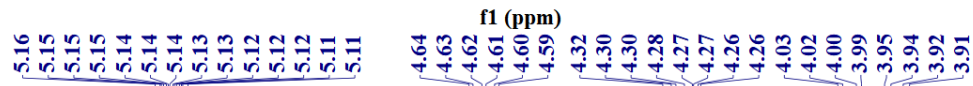


Fig. S5 GC analyses of the reaction mixture of the desired carbonate (2c) and minor amount of (3c).

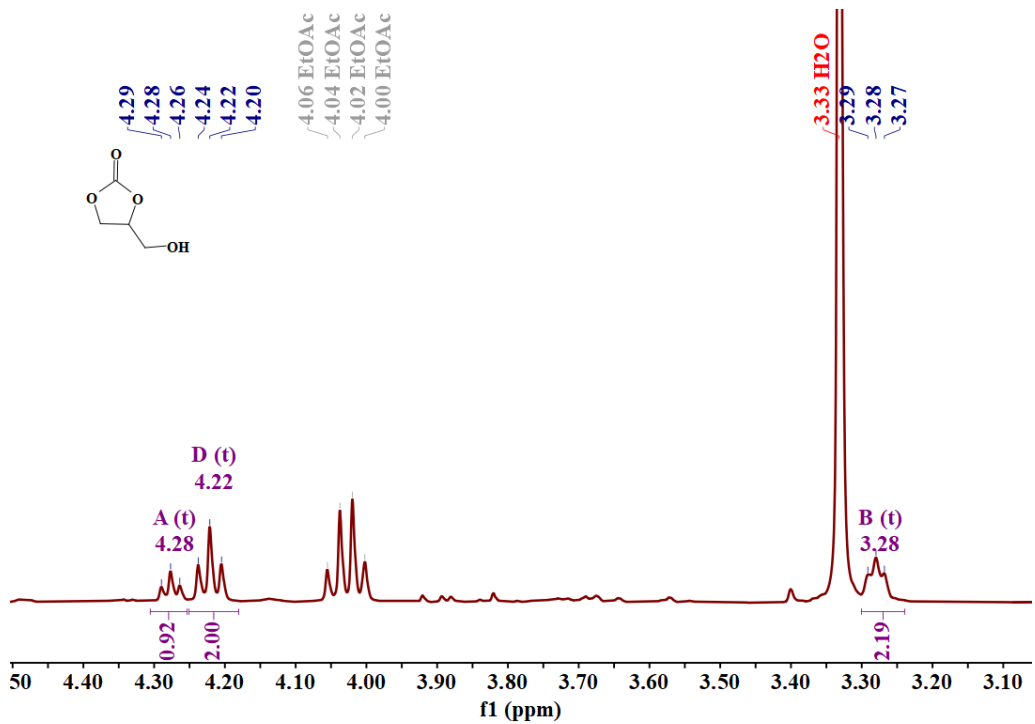
2b



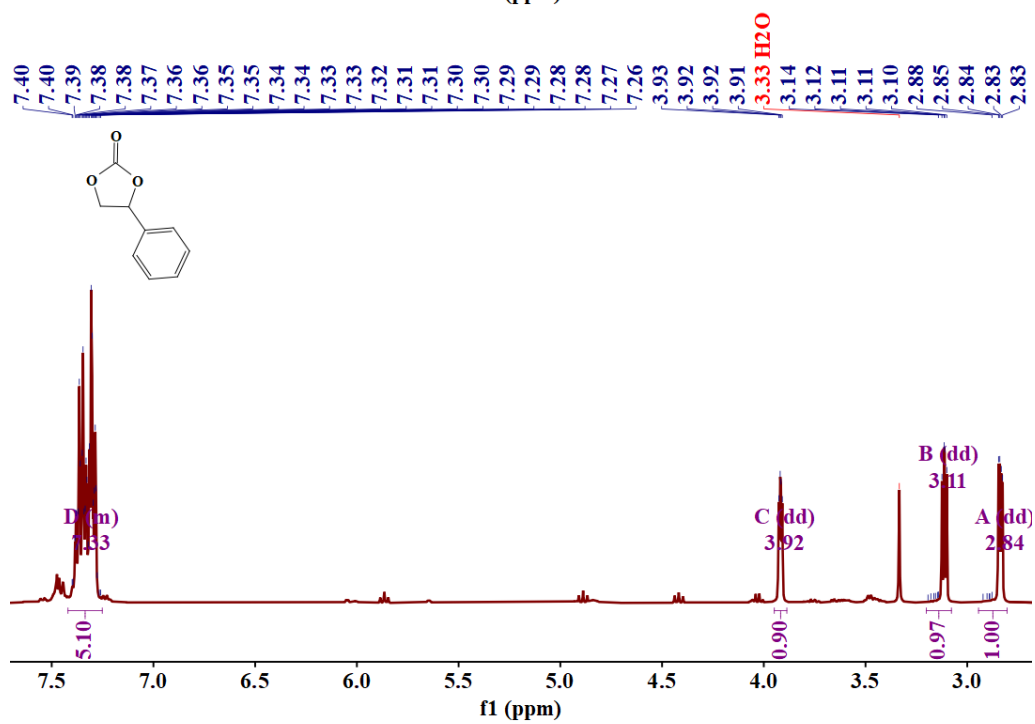
2c



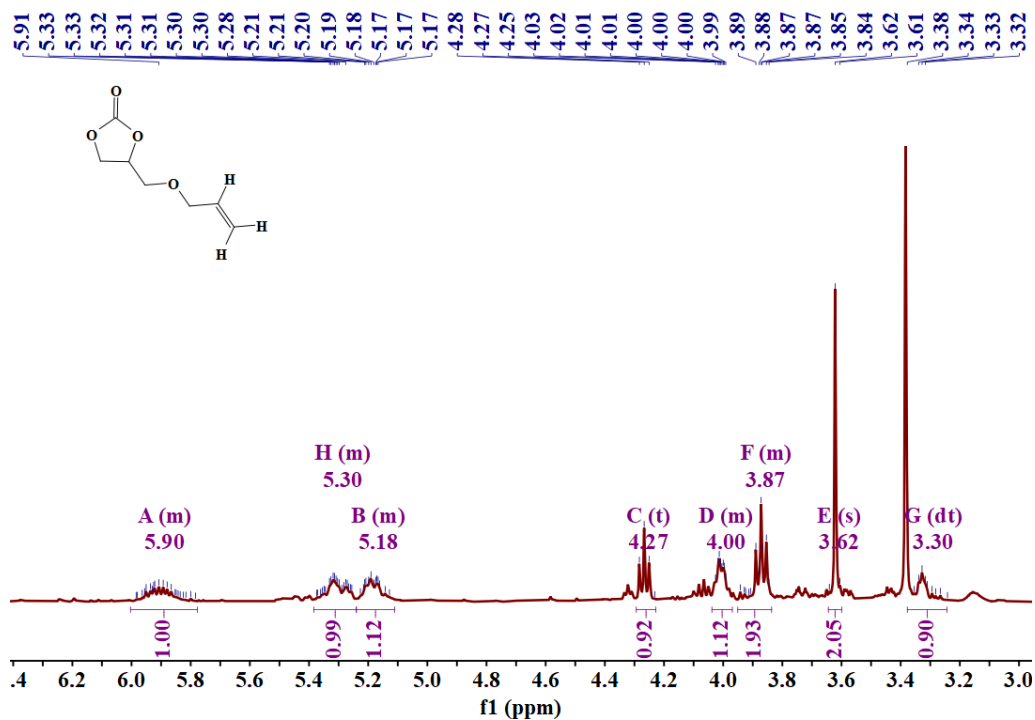
2d



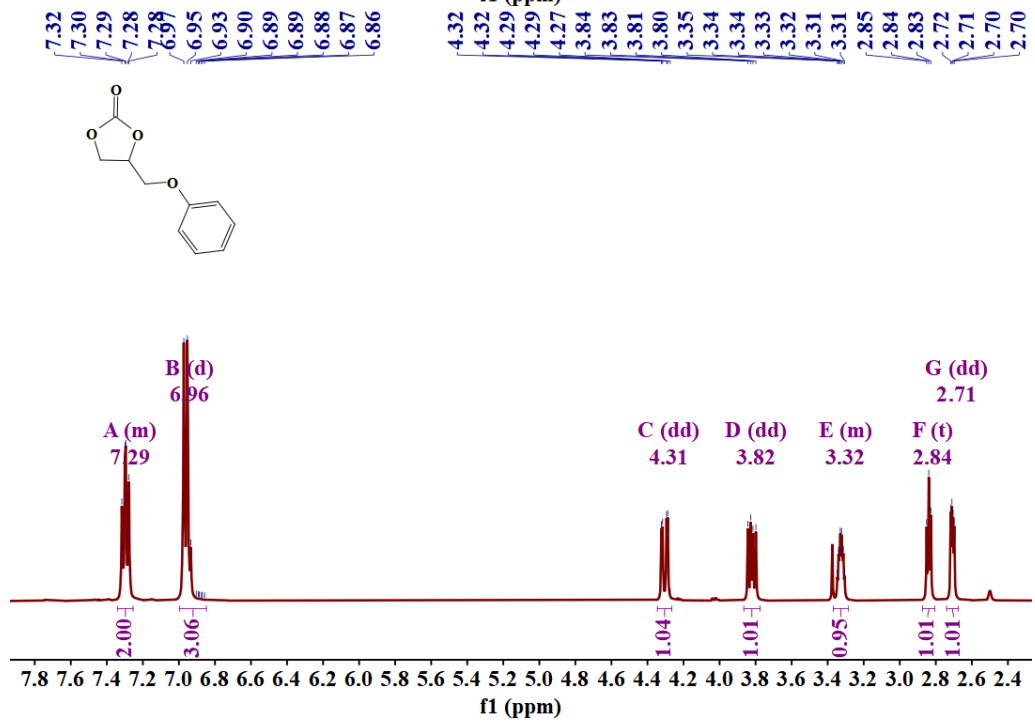
2e



2f



2g



2h

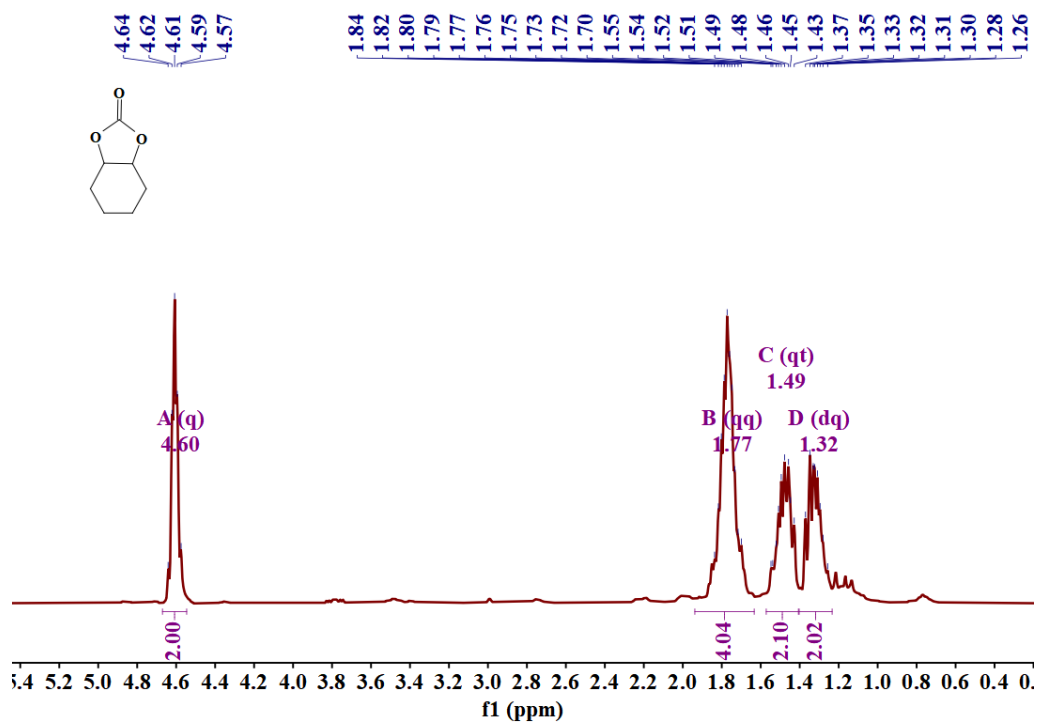


**Table S1** Catalytic performance of various catalysts.

Entry	Catalyst	Solvent	Epoxide	Conditions	Yield (%)
1	<b>ILPT</b>	None	ECH	Cat. 25 mol%, 30 °C, 0.1 MPa CO <sub>2</sub> (autoclave), 12 h	90.2
		1.25 mmol H <sub>2</sub> O	ECH	Cat. 25 mol%, 30 °C, 0.1 MPa CO <sub>2</sub> (autoclave), 12 h,	99.5
2 <sup>1</sup>	<b>ILW</b>	None	ECH	Cat. 15 mol%, 30 °C, 0.1 MPa CO <sub>2</sub> , 10 h	96.1
		5 mmol H <sub>2</sub> O	ECH	Cat. 15 mol%, 30 °C, 0.1 MPa CO <sub>2</sub> , 10 h	96.9
3 <sup>2</sup>	<b>ILH</b>	None	ECH	Cat. 25 mol%, 30 °C, 0.1 MPa CO <sub>2</sub> , 12 h	84
		2 mmol H <sub>2</sub> O	ECH	Cat. 25 mol%, 30 °C, 0.1 MPa CO <sub>2</sub> , 12 h	89
4 <sup>3</sup>	<b>DBPIL</b>	None	ECH	Cat. 6 mol%, 30 °C, 0.1 MPa CO <sub>2</sub> , 6 h	92
5 <sup>4</sup>	[HDBU]I	None	ECH	Cat. 10 mol%, 70 °C, 0.1 MPa CO <sub>2</sub> , 4 h	73.0
6 <sup>5</sup>	[TEA <sup>+</sup> O <sub>2</sub> <sup>-</sup> ][Br <sup>-</sup> ][DBUH <sup>+</sup> ]	None	PO	Cat. 15 mol%, 30 °C, 1.5 MPa CO <sub>2</sub> , 12 h	85
		None	PO	Cat. 15 mol%, 60 °C, 1.5 MPa CO <sub>2</sub> , 4 h	98
7 <sup>6</sup>	[Hmim] <sub>2</sub> [ZnBr <sub>4</sub> ]	None	ECH	Cat. 20 mol%, 25 °C, 0.1 MPa CO <sub>2</sub> , 5 h	99
8 <sup>7</sup>	Al-salen/[C <sub>1</sub> C <sub>4</sub> Im][HCO <sub>3</sub> ]	None	SO	Cat. 0.25 mol%, 25 °C, 1 MPa CO <sub>2</sub> , 10 h	58
9 <sup>8</sup>	Zn-Salen-COF-SDU113	None	PO	25 °C, 1atm CO <sub>2</sub> , 48 h	97.3
10 <sup>9</sup>	CuBDC-CMC/TBAB	None	ECH	Cat. 0.5 mol%, 70 °C, 1atm CO <sub>2</sub> , 18 h	91.1
11 <sup>10</sup>	SBA-Zn-TPy <sup>+</sup> PI <sup>-</sup> <sub>DMF</sub>	None	PO	Cat. 0.1 mol%, 120 °C, 1.5 MPa CO <sub>2</sub> , 3.5 h	99
12 <sup>11</sup>	PEAMC1	None	SO	Cat. 0.1g, 120 °C, 10 bar CO <sub>2</sub> , 3 h	92.4

### 3. Theoretical Section

The structures of all reactants, products, intermediates, and transition states were optimized by the Becke's three parameter exact exchange functional combined with Perdew and Wang (B3PW91)<sup>12,13</sup> method with the 6-31G(d,p) basis set.<sup>14</sup> Simultaneously, the vibration frequency of the harmonic vibration was calculated at the same level. The transition state has only one imaginary frequency, and the minimum has no imaginary frequency. The minimum-energy path (MEP) was obtained by the intrinsic reaction coordinate (IRC) method<sup>15</sup> starting from the transition state. The energies were corrected at the M06/6-311+G(2d,2p) level<sup>16</sup> on the basis of the geometries optimized at the B3PW91/6-31G(d,p) level. And the solvent effect was taken into consideration by the polarized continuum model (PCM) in ethyl ether (Et<sub>2</sub>O) solvent.<sup>17,18</sup> Aforementioned all calculations were performed by the Gaussian 09 program package.<sup>19</sup> Insight into the topological properties and the nature of the interactions, atoms in molecule (AIM) analysis,<sup>20,21</sup> non-covalent interaction (NCI)<sup>22</sup> and electron localization function (ELF)<sup>23,24</sup> were performed using the Multiwfn 3.6 program.<sup>25</sup> The results are presented in Table S2, Figs. 4 and Figs. S7-S15. The detailed definitions for AIM, NCI, and ELF refer to refs. 20-24.

Seven possible pathways are considered for this reaction catalyzed by **ILPT** (See Fig. 4, Figs. S9-11, and Figs. S13-S15). For Route 1, CO<sub>2</sub> would be attracted by -COO<sup>-</sup> group. Then, H1 atom in [TMGH<sup>+</sup>] group of **ILPT** would be employed as electrophile to promote the ring-opening of ECH with the rate-determining barrier height of 18.2 kcal mol<sup>-1</sup> (See Fig. S9). As to Route 6 (See Fig. S14), the coupling reaction still follows the traditional three step mechanism, ring-opening of ECH prompted by both H1 atom in [TMGH<sup>+</sup>] group and Br<sup>-</sup> anion, CO<sub>2</sub> addition, and ring-closure to form the final products. The barrier heights of rate-determining step for



Route 1 (18.2 kcal mol<sup>-1</sup>) and Route 6 (18.5 kcal mol<sup>-1</sup>) are close to each other indicating that they are competing routes. Alternatively, ECH, CO<sub>2</sub>, and **ILPT** would firstly form an intermediate (See Fig. S15), CP7-1, by hydrogen bond. After that, the C atom of CO<sub>2</sub> activate the ECH along with the nucleophilic activation from Br<sup>-</sup> anion leading to the ring-opening of ECH, which is Route 7 with the rate-determining barrier height of 28.8 kcal mol<sup>-1</sup>.

In aforementioned three pathways, the ring-opening of ECH is the rate-determining step with the highest barrier height. Moreover, all of them are the larger than that of route W3 in Fig. S7, which is consistent with the less activity of **ILPT** without water.

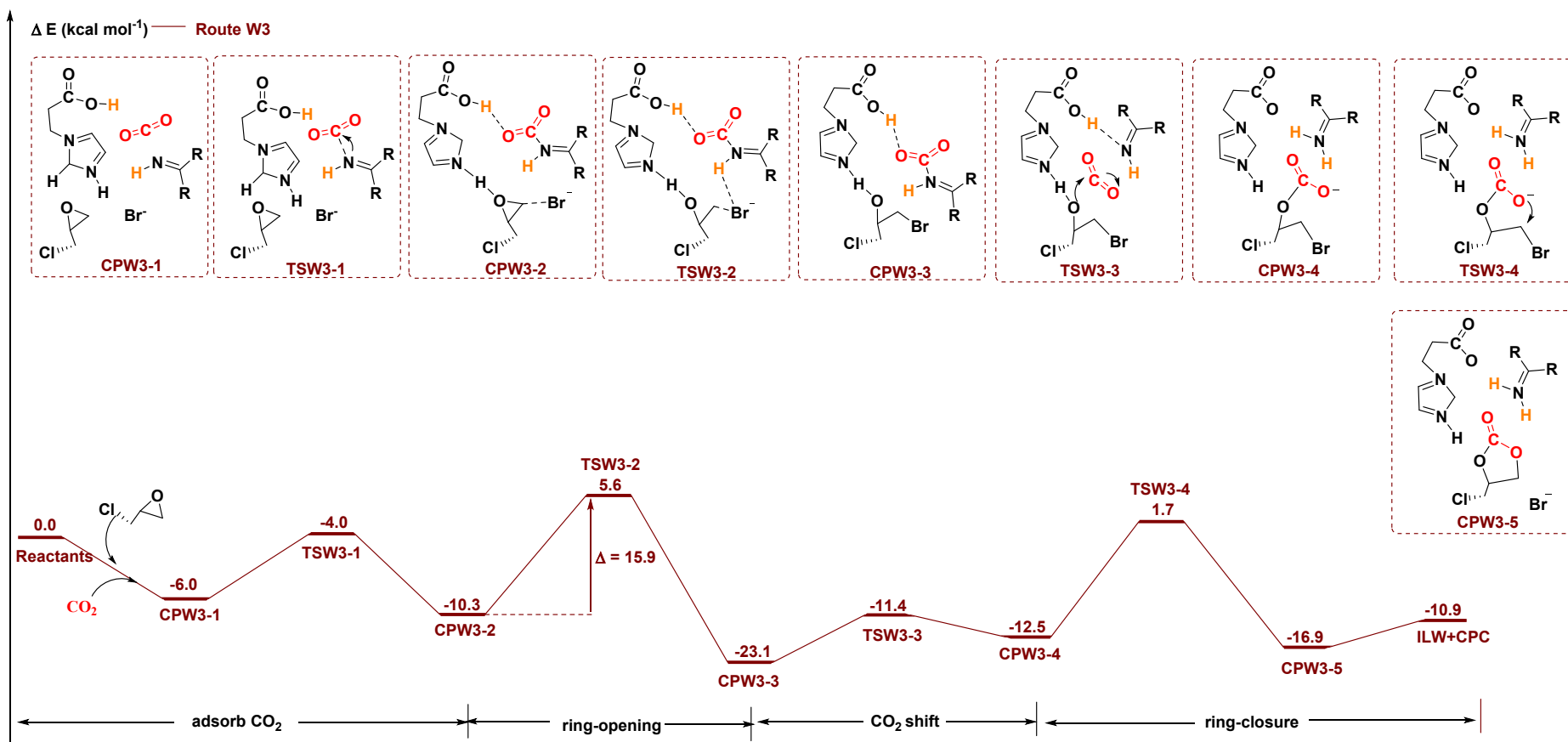


**Fig. S7** The optimized geometries of all transition states and intermediates involved in Route W3 together with the corresponding potential energy profile calculated at the M06/6-311+G(2d,2p) (PCM)//B3PW91/6-31 G(d,p) level. The zero is defined as the sum energy of the separate reactant and ILW from literature<sup>1</sup>.

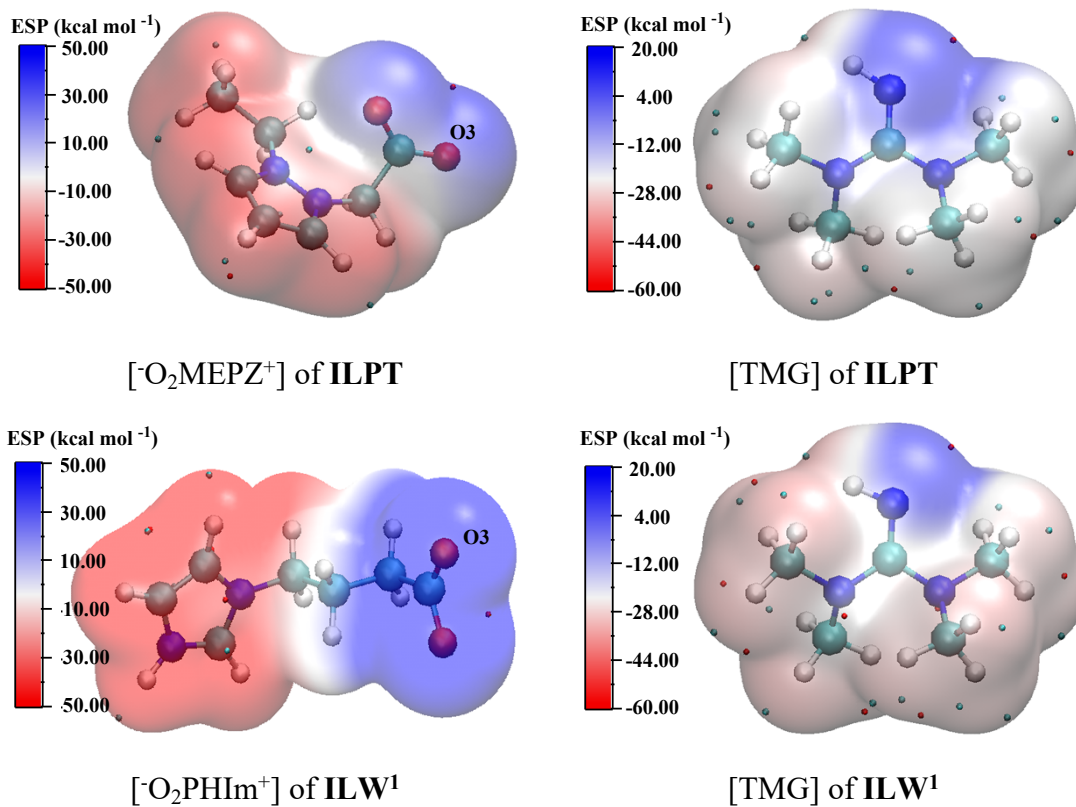


**Fig. S8** The ESP mapped onto a surface of electron distribution for the studied ionic liquids. Blue colour represents the negative electrostatic potential and red colour represents the positive electrostatic potential.

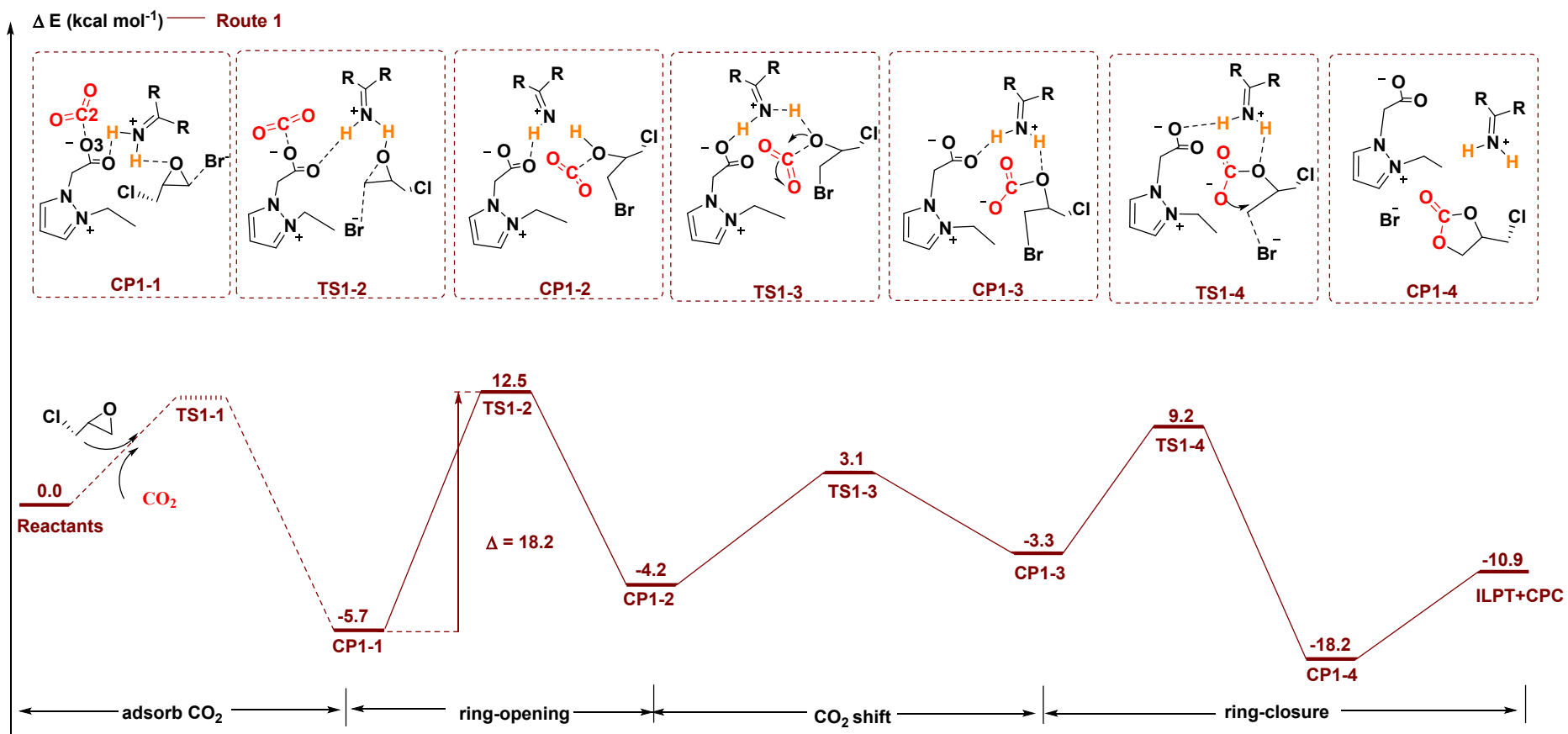


**Fig. S9** The optimized geometries of all transition states and intermediates involved in Route 1 together with the corresponding potential energy profile calculated at the M06/6-311+G(2d,2p) (PCM)//B3PW91/6-31 G(d,p) level. The zero is defined as the sum energy of the separate reactant and **ILPT**.

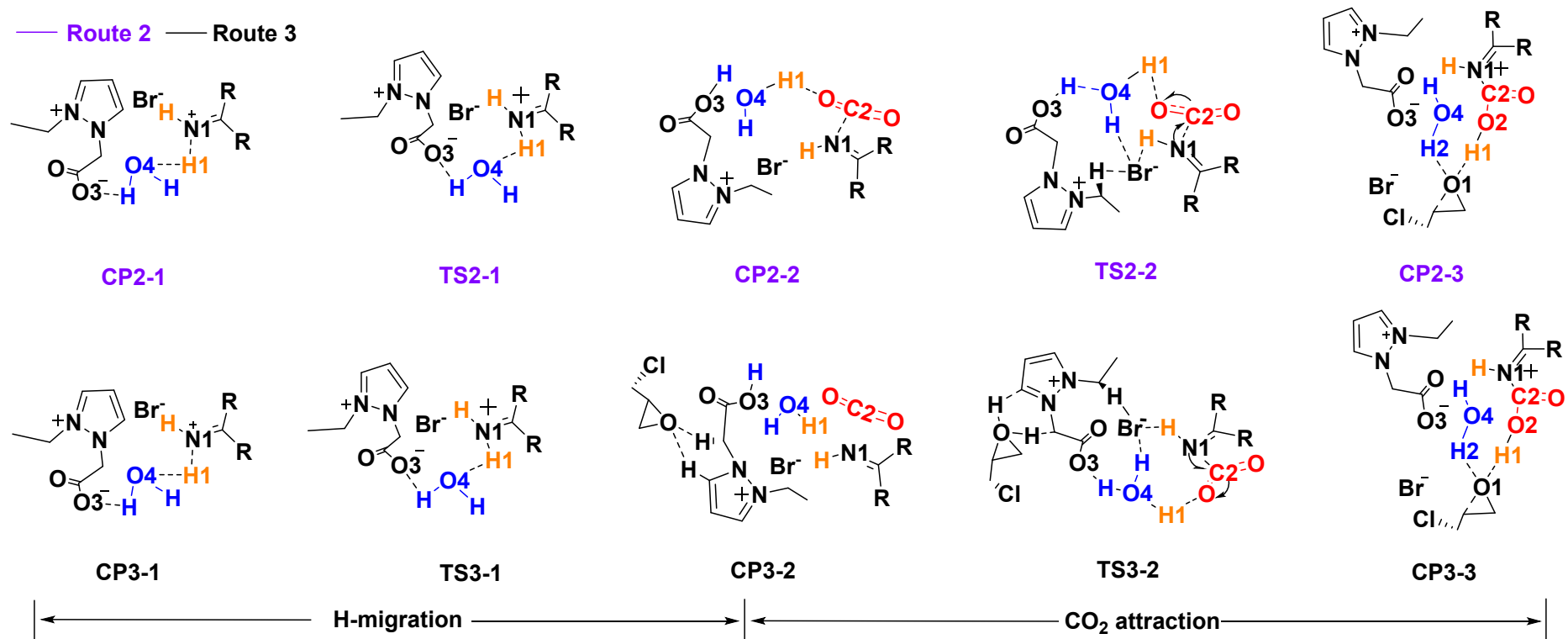
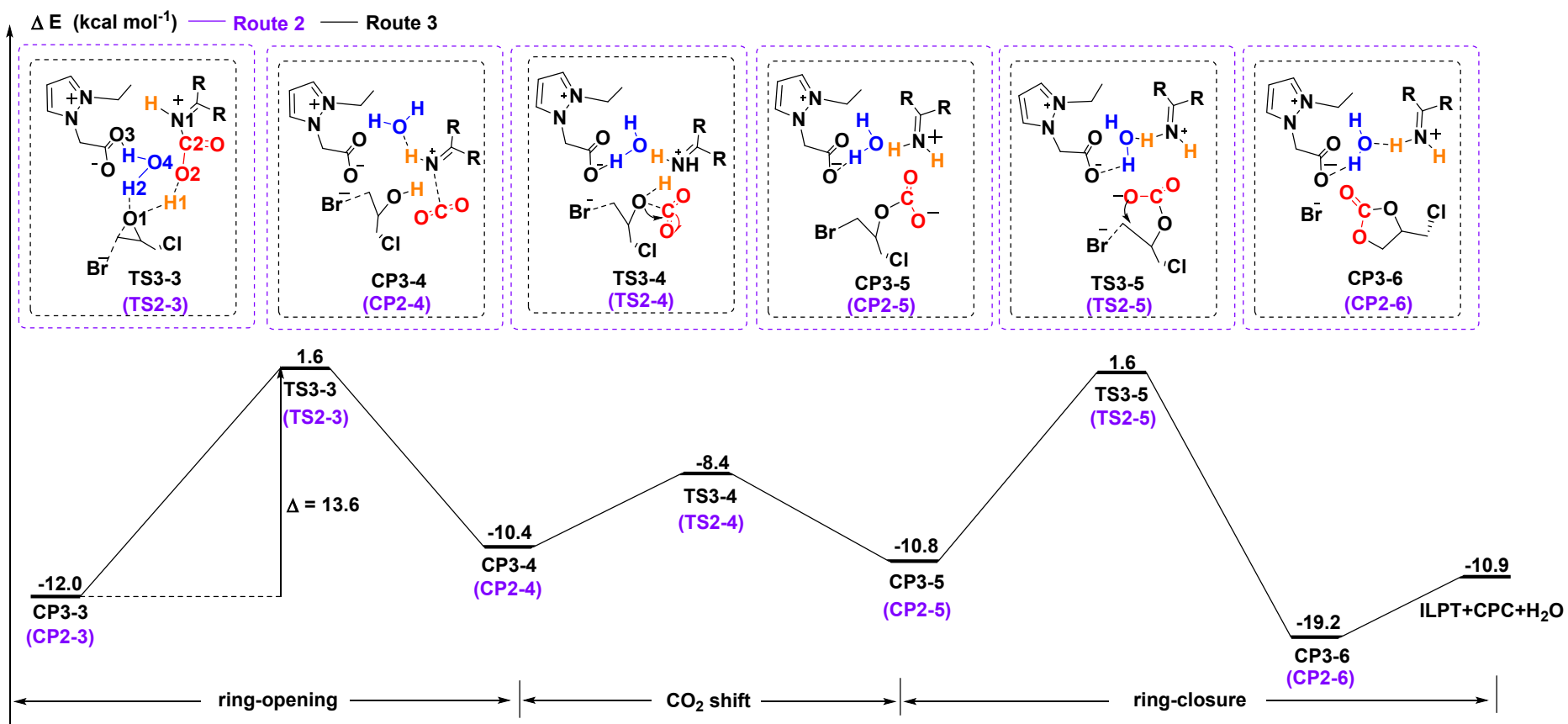
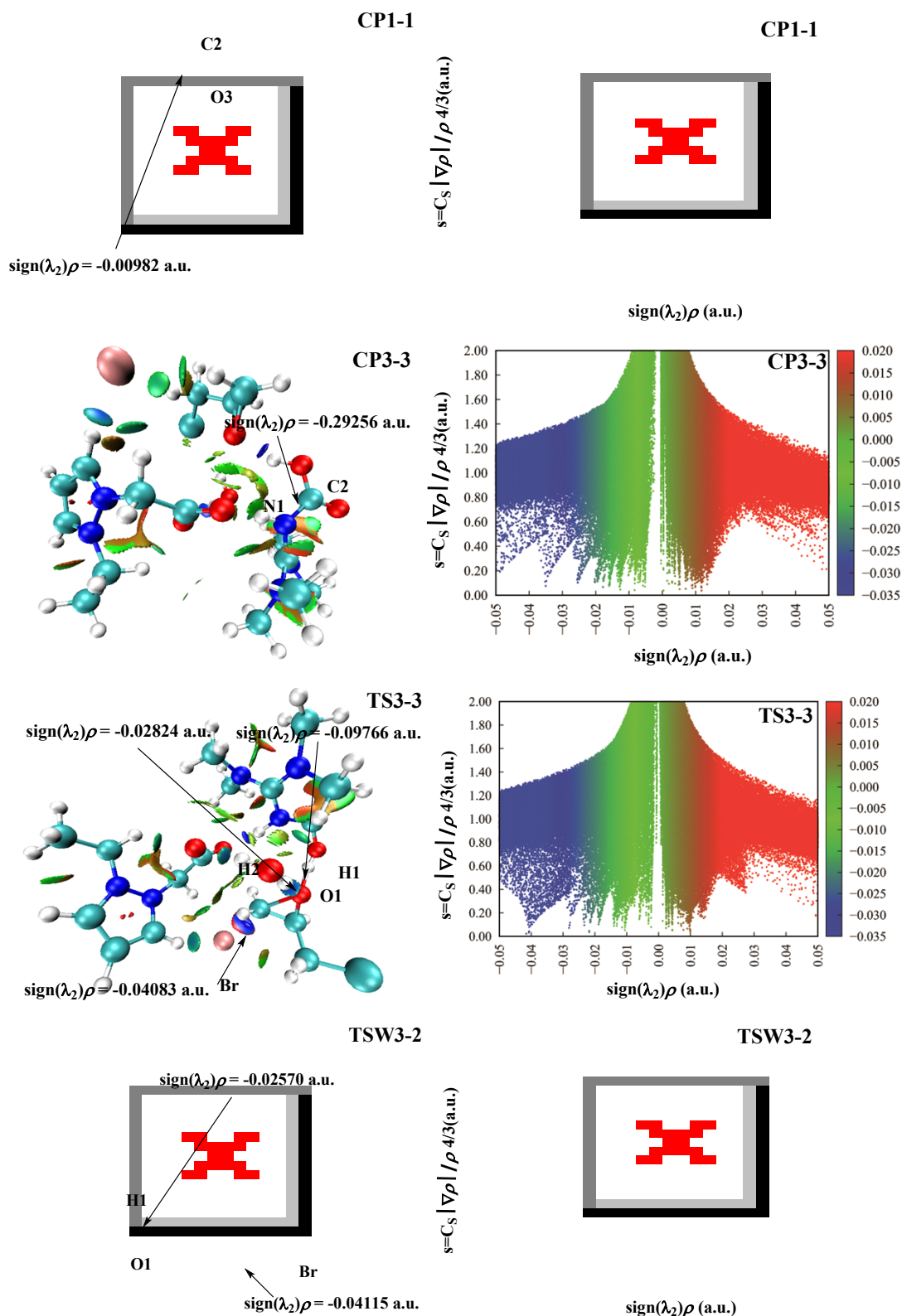


Fig. S10 The optimized geometries of some transition states and intermediates involved in Route 2 and Route 3.

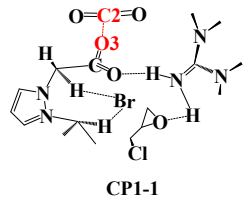
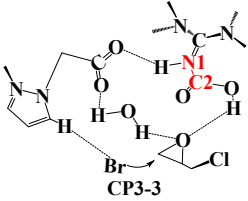
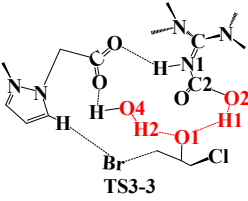
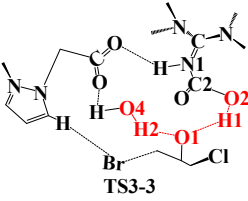


**Fig. S11** The optimized geometries of some transition states and intermediates involved in Route 2 and Route 3 together with the corresponding potential energy profile calculated at the M06/6-311+G(2d,2p) (PCM)/B3PW91/6-31G(d,p) level. The zero is defined as the sum energy of the separate reactant and ILPT.



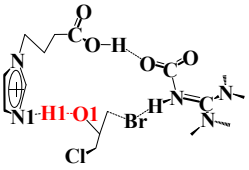
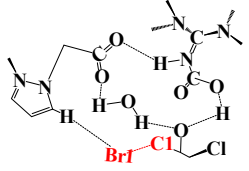
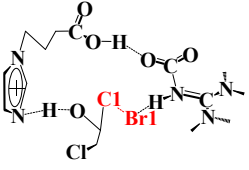
**Fig. S12** NCI plots for CP1-1 (ILPT), CP3-3 (ILPT), TS3-3 (ILPT), and TSW3-2 (ILW)<sup>1</sup>. The corresponding 3D plots are displayed left with blue regions representing strong electrostatic interactions and green regions representing more dispersive attractive interactions.

**Table S2.** Selected topological parameters of the BCPs in the CO<sub>2</sub> absorption step and ring-opening step calculated at the B3PW91/6-31G(d,p) level of theory in Route 1 (ILPT), Route 3 (ILPT), and Route W3 (ILW).

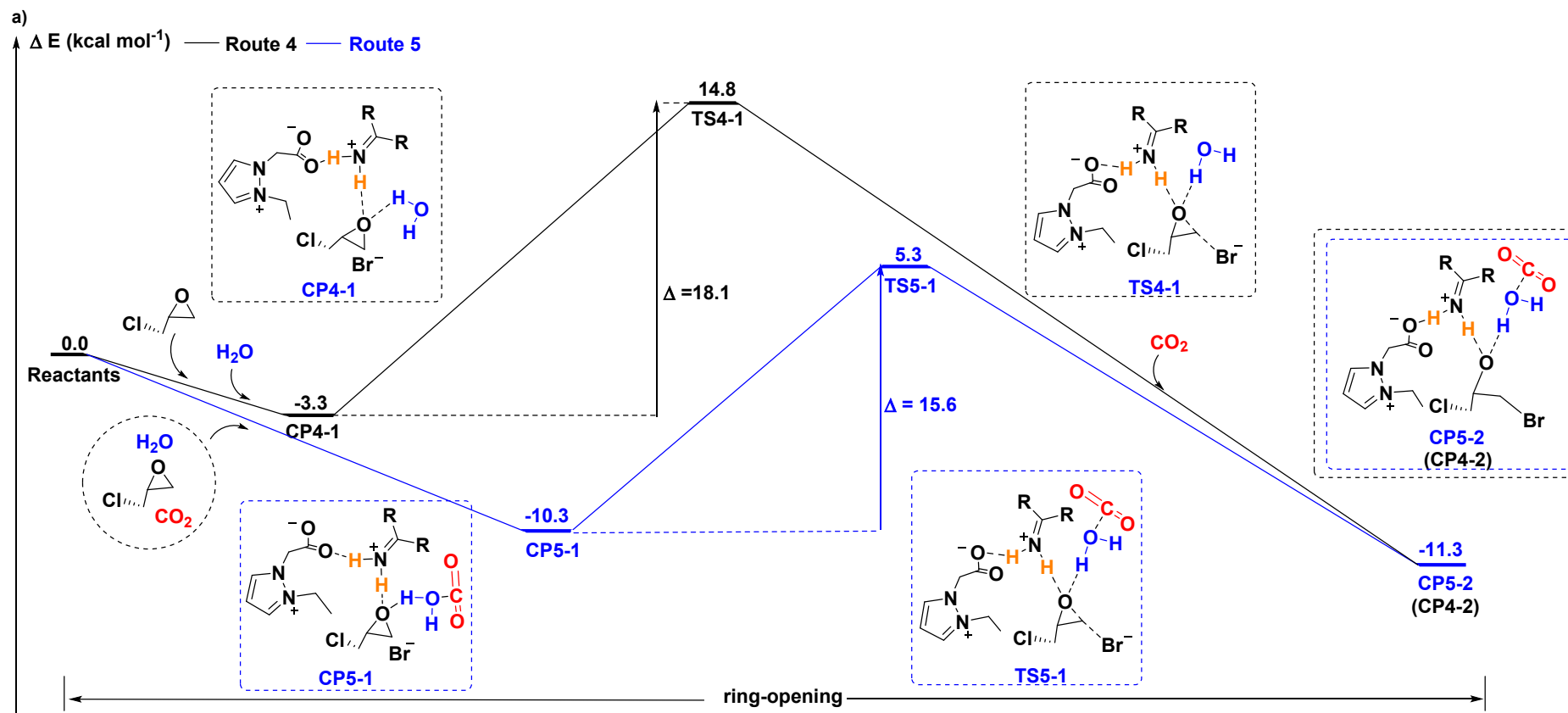
Reaction steps	X-Y...Z	Ionic Liquids	Intermediate/ Transition state	Sign( $\lambda_2$ ) $\rho$	$\rho$	$\nabla^2\rho$	G	V	H
CO <sub>2</sub> absorption step	C2...O3	ILPT	 CP1-1	-0.00982	0.00982	0.04013	0.00854	-0.00704	0.00149
	C2...N1	ILPT	 CP3-3	-0.29256	0.29256	-0.93875	0.15108	-0.53685	-0.38577
Ring-opening step	H1...O1	ILPT	 TS3-3	-0.09766	0.09766	0.11221	0.06980	-0.11155	-0.04175
	H2...O1	ILPT	 TS3-3	-0.02824	0.02824	0.08007	0.02097	-0.02192	-0.00095



---

H1...O1	<b>ILW<sup>1</sup></b>	 <p>TSW3-2</p>	-0.15918	0.15918	-0.28449	0.08863	-0.24837	-0.15975
Br1...C1	<b>ILPT</b>	 <p>TSW3-3</p>	-0.04083	0.04083	0.07045	0.02116	-0.02470	-0.00354
Br1...C1	<b>ILW<sup>1</sup></b>	 <p>TSW3-2</p>	-0.03573	0.03573	0.06890	0.01920	-0.02118	-0.00198

---



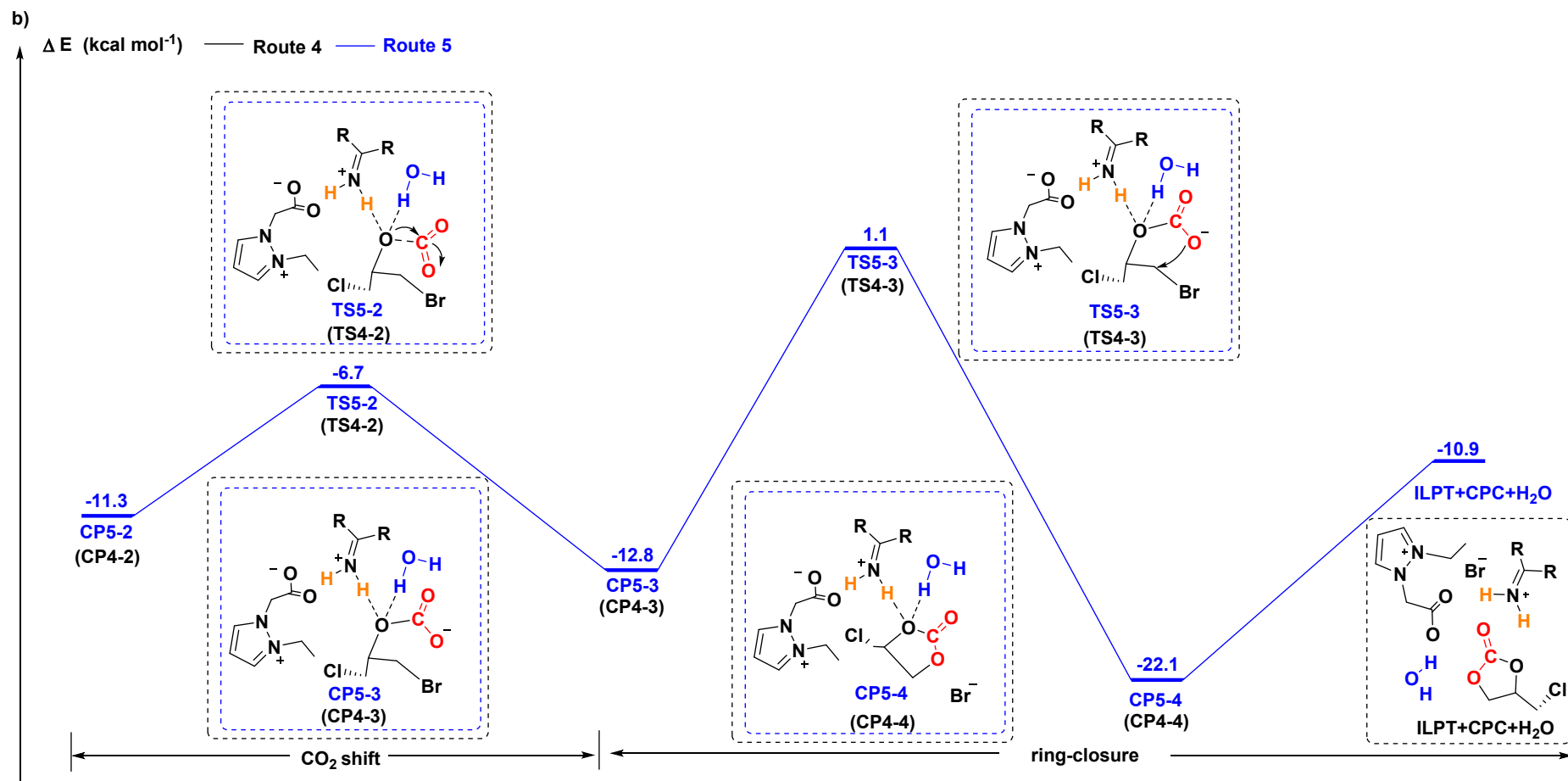


**Fig. S13** The optimized geometries of all transition states and intermediates involved in Route 4 and Route 5 together with the corresponding potential energy profile calculated at the M06/6-311+G(2d,2p) (PCM)/B3PW91/6-31 G(d,p) level. The zero is defined as the sum energy of the separate reactant and ILPT.

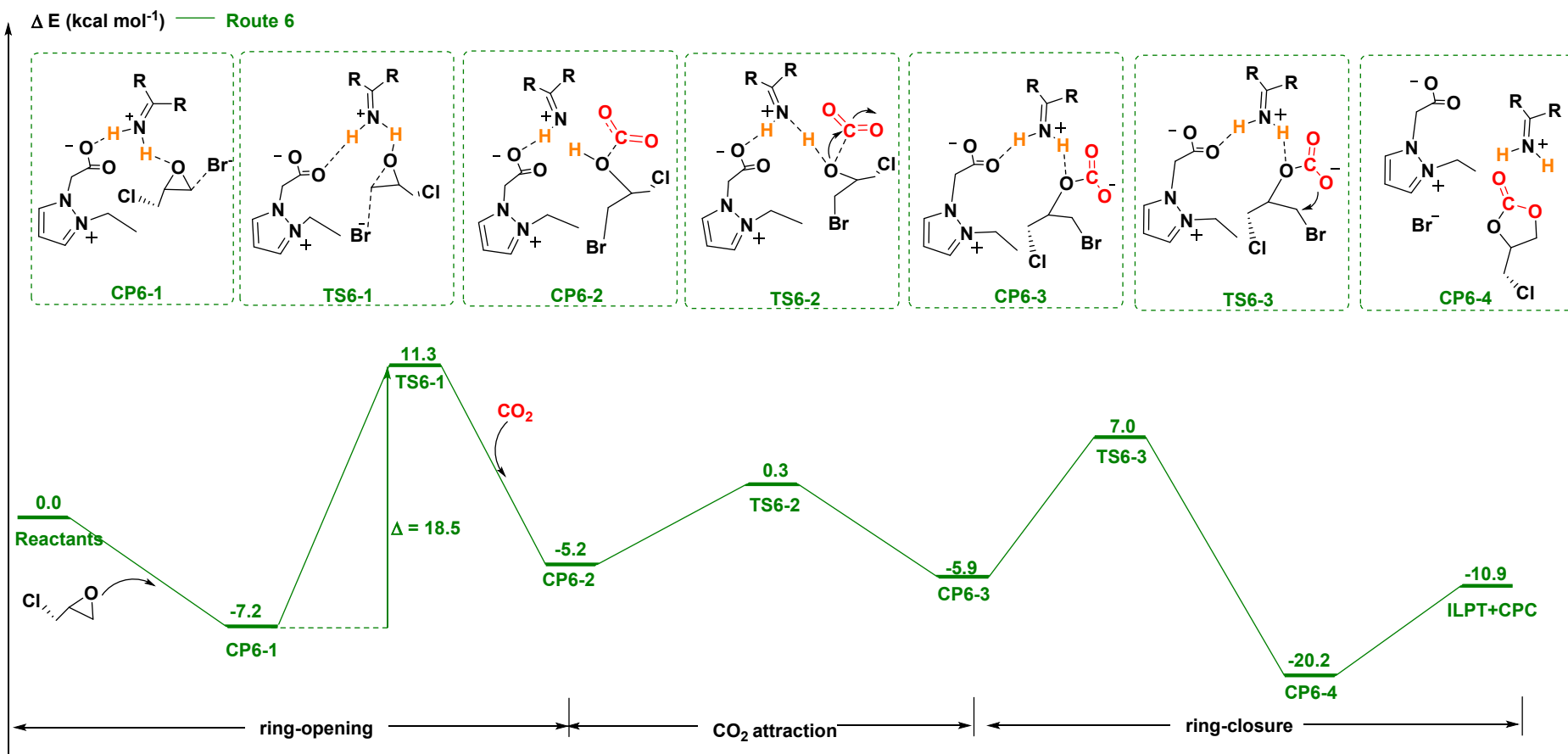


**Fig. S14** The optimized geometries of all transition states and intermediates involved in Route 6 together with the corresponding potential energy profile calculated at the M06/6-311+G(2d,2p) (PCM)//B3PW91/6-31 G(d,p) level. The zero is defined as the sum energy of the separate reactant and ILPT.

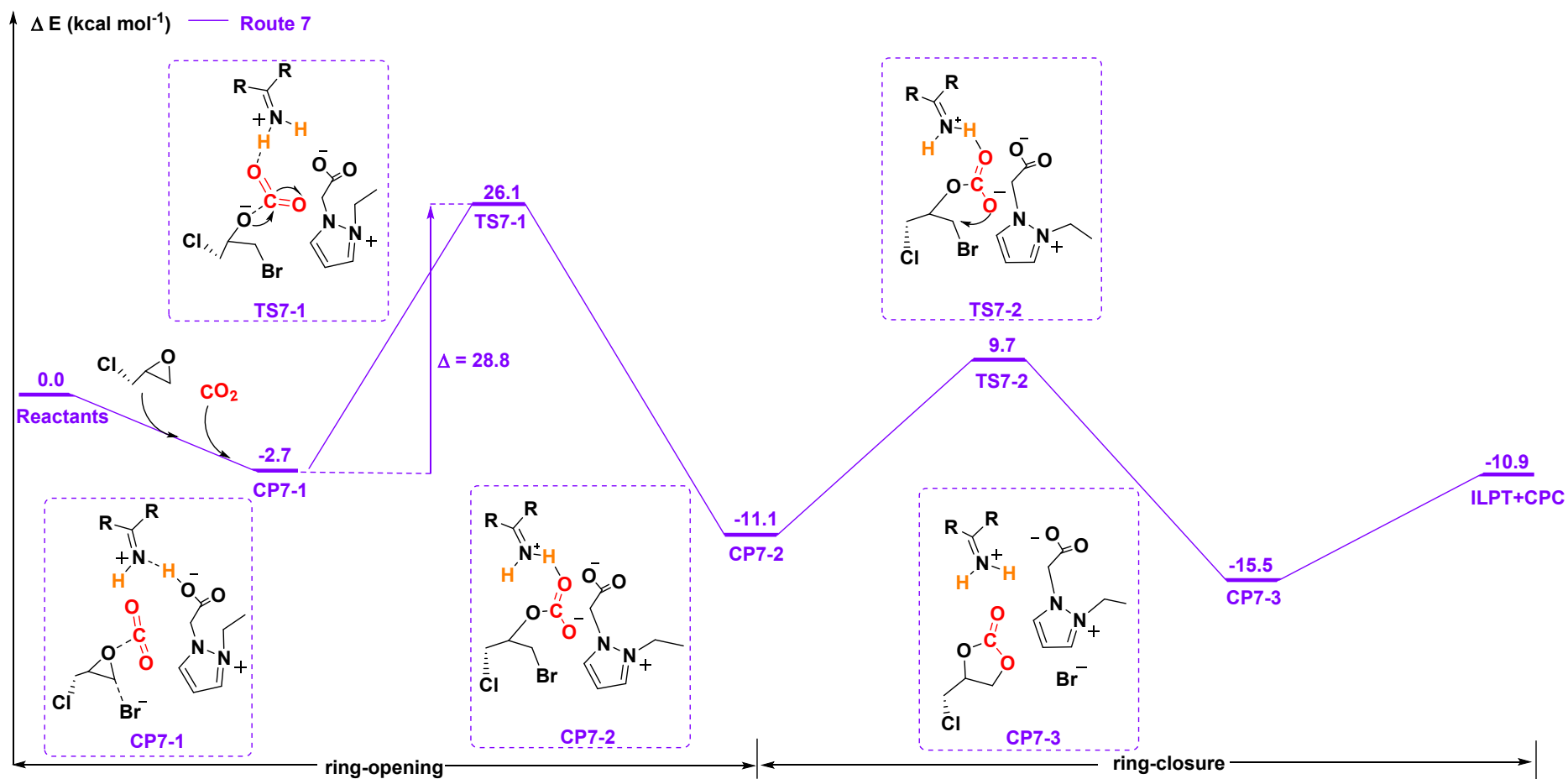


**Fig. S15** The optimized geometries of all transition states and intermediates involved in Route 7 together with the corresponding potential energy profile calculated at the M06/6-311+G(2d,2p) (PCM)//B3PW91/6-31 G(d,p) level. The zero is defined as the sum energy of the separate reactant and ILPT.

## References

- [1] T.F. Wang, D.N. Zheng, B.B. An, Y. Liu, T.G. Ren, H. Ågren, L. Wang, J.L. Zhang and M.S.G. Ahlquist, *Green Energy Environ.*, 2021, 10.1016/j.gee.2021.02.011.
- [2] J.Y. Hu, J. Ma, H.Z. Liu, Q.L. Qian, C. Xie and B.X. Han, *Green Chem.*, 2018, **20**, 2990-2994.
- [3] X.L. Meng, Z.Y. Ju, S.J. Zhang, X.D. Liang, N.V. Solms, X.C. Zhang and X.P. Zhang, *Green. Chem.*, 2019, **21**, 3456-3463.
- [4] N. Fanjul-Mosteirín, C. Jehanno, F. Ruipérez, H. Sardon and A.P. Dove, *ACS Sustain. Chem. Eng.*, 2019, **7**, 10633-10640.
- [5] F.S. Liu, Y.Q. Gu, P.H. Zhao, J. Gao and M.S. Liu, *ACS Sustain. Chem. Eng.*, 2019, **7**, 940-5945.
- [6] G. Chen, J.L. Zhang, X.Y. Cheng, X.N. Tan, J.B. Shi, D.X. Tan, B.X. Zhang, Q. Wan, F.Y. Zhang, L.F. Liu, B.X. Han, G.Y. Yang, *Chemcatchem*, 2020, **12**, 1963-1967.
- [7] J. Liu, G. Yang, Y. Liu, D. Zhang, X. Hu and Z. Zhang, *Green Chem.*, 2020, **22**, 4509-4515.
- [8] W. Zhou, Q.W. Deng, G.Q. Ren, L. Sun, L. Yang, Y.M. Li, D. Zhai, Y.H. Zhou and W.Q. Deng, *Nat. Commun.*, 2020, **11**, 1-9.
- [9] X.J. Bai, X.Y. Lu, R. Ju, H. Chen, L. Shao, X. Zhai, X. Zhai, Y.N. Li, F. Q. Fan, Y. Fu and W. Qi, *Angew. Chem. Int. Ed.*, 2021, **60**, 701-705.
- [10] S. Jayakumar, H. Li, L. Tao, C.Z. Li, L. Liu, J. Chen and Q.H. Yang, *ACS*

*Sustain. Chem. Eng.*, 2018, **6**, 9237-9245.

[11] X.C. Wang , Q. Dong , Z.Z. Xu , Y. Wu , D.M. Gao , Y.S. Xu , C.J. Ye , Y.T.

Wen , A.Q. Liu , Z.Y. Long and G.J. Chen, *Chem. Eng. J.*, 2021, **403**, 126460.

[12] A.D. Becke, *J. Chem. Phys.*, 1993, **98**, 5648-5652.

[13] J.P. Perdew, K. Burke and Y. Wang, *Phys. Rev. B*, 1996, **54**, 16533.

[14] P.M.W. Gill, B.G. Johnson, J.A. Pople and M.J. Frisch, *Chem. Phys. Lett.*, 1992,

**197**, 499-505.

[15] K. Fukui, *J. Phys. Chem.*, 1970, **74**, 4161-4163.

[16] Y Zhao and D.G. Truhlar., *Theor. Chem. Acc.*, 2008, **120**, 215-241.

[17] S. Miertuš, E. Scrocco and J. Tomasi, *Chem. Phys.* 1981, **55**, 117-129.

[18] S. Miertus and J. Tomasi, *Chem. Phys.*, 1982, **65**, 239-245.

[19] M.J. Frisch, G.W. Trucks, H.B. Schlegel, G.E. Scuseria, M.A. Robb, J.R.

Cheeseman, G. Scalmani, V. Barone, B. Mennucci, G.A. Petersson, H. Nakatsuji,

M. Caricato, X. Li, H.P. Hratchian, A.F. Izmaylov, J. Bloino, G. Zheng, J.L.

Sonnenberg, M. Hada, M. Ehara, K. Toyota, R. Fukuda, J. Hasegawa, M. Ishida,

T. Nakajima, Y. Honda, O. Kitao, H. Nakai, T. Vreven, J.A. Montgomery, Jr., J.E.

Peralta, F. Ogliaro, M. Bearpark, J.J. Heyd, E. Brothers, K.N. Kudin, V.N.

Staroverov, T. Keith, R. Kobayashi, J. Normand, K. Raghavachari, A. Rendell,

J.C. Burant, S.S. Iyengar, J. Tomasi, M. Cossi, N. Rega, J.M. Millam, M. Klene,

J.E. Knox, J.B. Cross, V. Bakken, C. Adamo, J. Jaramillo, R. Gomperts, R.E.

Stratmann, O. Yazyev, A.J. Austin, R. Cammi, C. Pomelli, J.W. Ochterski, R.L.

Martin, K. Morokuma, V.G. Zakrzewski, G.A. Voth, P. Salvador, J.J.

Dannenberg, S. Dapprich, A.D. Daniels, O. Farkas, J.B. Foresman, J.V. Ortiz, J. Cioslowski, D.J. Fox, Gaussian 09, Revision A.02, Gaussian Inc. Wallingford, CT, 2009.

[20] R.F.W. Bader and P.M. Beddall, *J. Chem. Phys.*, 1972, **56**, 3320-3329.

[21] U. Koch and P.L.A. Popelier, *J. Phys. Chem.*, 1995, **24**, 9747-9754.

[22] E.R. Johnson, S. Keinan, P. Mori-Sánchez, J. Contreras-García, A.J. Cohen and W. Yang, *J. Am. Chem. Soc.*, 2010, **132**, 6498-6506.

[23] A. Savin, R. Nesper, S. Wengert and T.F. Fässler, *Angew. Chem. Int. Ed.*, 1997, **36**, 1808-1832.

[24] J. Poater, M. Duran, M. Sola and B. Silvi, *Chem. Rev.*, 2005, **105**, 3911-3947.

[25] T. Lu and F. Chen, *J. Comput. Chem.*, 2012, **33**, 580-592.